

Process based virtual rhizotron experiments to investigate the impact of maize roots on ERT derived effective electrical conductivity of the soil-root continuum

Sathyanarayan Rao¹, Félicien Meunier², Solomon Ehosioko³, Nolwenn Lesparre⁴, Andreas Kemna⁵, Frédéric Nguyen³, Sarah Garré⁶, Mathieu Javaux^{1,7}.

¹ Université catholique de Louvain, Earth and Life Institute-Environmental Sciences, Louvain-la-Neuve, Belgium

² Computational and Applied Vegetation Ecology lab, Ghent University, Gent, Belgium

³ Applied Geophysics, Université de Liège, Chemin des Chevreuils 1, 4000 Liege, Belgium

⁴ Laboratoire d'Hydrologie et Géochimie de Strasbourg, University of

Strasbourg/EOST/ENGES, CNRS UMR 7517, 1 Rue Blessig, 67084 Strasbourg, France

⁵ Department of Geophysics, University of Bonn, Meckenheimer Allee 176, 53115 Bonn, Germany

⁶ Université de Liège, Gembloux Agro-Bio Tech, TERRA Research and Teaching Center, Passage des déportés 2, 5030 Gembloux, Belgium.

⁷ Agrosphere, IBG3, Forschungszentrum Juelich GmbH, Germany

Correspondence to : Mathieu Javaux (mathieu.javaux@uclouvain.be)

Abstract

Electrical Resistivity Tomography (ERT) has become an important tool to study soil water fluxes in cropped field. ERT results translate to water content via empirical pedophysical relations that take soil physical properties into account, usually ignoring the impact of roots. Studies show that high root dense soils behave quite differently than less root dense soils in terms of bulk electrical conductivity. Yet, we do not completely understand the impact of root segments on the ERT measurements. In this numerical study, we coupled an electrical model with a plant-soil water flow model to investigate the impact of root growth and water uptake on virtual ERT measurements. The coupled model can simulate root growth and development (including changes of root electrical properties with aging), water flow in soil and root systems, as well as electrical transfer in the soil-root continuum and hence reproduce ERT experiments. The electrical properties of roots are explicitly accounted for in the finite element mesh. We obtained the electrical conductivities of root segments to parameterize the model by measuring electrical conductivity on real maize plants. The contrast between electrical conductivity of roots and soil depends on factors such as root density, irrigation, root age, and root water uptake pattern. Therefore, root growth and water uptake processes affect this contrast together with the soil electrical properties. In this study, we illustrate the developed model by an ERT numerical experiment applied to a 2D rhizotron planted with 3-weeks old maize. Model results indicate a non-negligible anisotropy in bulk electrical conductivity induced by root processes. We see a greater anisotropy in a sandy medium when compared to a loamy medium. Root water uptake processes dominate the bulk electrical properties. The Gauss-Newton type ERT inversion of virtual rhizotron data demonstrate that, when root-soil electrical conductivity contrasts are high, it can lead to error in water content estimates since the electrical conductivity is partly due to the presence of roots. Thus, incorporating the impact of roots in the pedophysical relations is important to interpret ERT results. The process-based model presented in this study is suited to analyze the impact of roots on the electrical signal in any condition and to better interpret experimental ERT data.

1 Introduction

Understanding root water uptake and associated nutrients is critical for crop management (e.g. Gregory et al. 2005) but remains a challenging task due to the inherent difficulty to collect observations in the soil (e.g. de Dorlodot et al., 2007). Geophysical monitoring of soil-root system water fluxes have received growing interest in the past decades to tackle this challenge. In particular, in this paper, we will investigate the potential of Electrical Resistivity Tomography (ERT) to map changes in water content in a rhizotron. ERT aims at retrieving the 2D or 3D distribution of the electrical conductivity (σ) or its inverse resistivity in the soil. The electrical conductivity is then related to the variable of interest (for instance the soil water content SWC) through a pedophysical relationship.

In cropped fields, ERT has been increasingly used for monitoring soil water content (SWC) (Beff et al., 2013; Brillante et al., 2016; De Carlo et al., 2015; Garré et al., 2013; Michot et al., 2003; Srayeddin and Doussan, 2009; Vanella et al., 2018). More recently, ERT-estimated water content was used for phenotyping root systems at field scale (Whalley et al., 2017). The authors monitored changes in σ of the soil root zone in drying condition at different soil depths, which acted as a proxy of root activity. However, bulk conductivity of a vegetated soil (potentially containing roots), denoted by σ_{bulk} , and does not only depend on SWC, but also on roots and their impact on soil structure. Field experiments further show that the rooted zone soil behaves quite different in terms of pedophysical relation as compared to soil containing no roots (Michot et al., 2016; Werban et al., 2008). Therefore ERT-monitored SWC in agricultural fields can be inaccurate or misleading if we ignore the impact of root-related processes on the bulk conductivity of the soil-root continuum.

In the literature, various studies mention or even target the impact of roots on σ_{bulk} . In Fig. 1, we report values of bulk soil electrical conductivity without roots, denoted by $\sigma_{bulk-soil}$, and root segment electrical conductivity, denoted by σ_{root} . The ratio between σ_{root} and $\sigma_{bulk-soil}$ is generally a function of plant species, soil type, SWC and solute concentration.

For a given species, σ_{root} is a function of root anatomy, which can be related to root age, root order or root diameter. In their study, Anderson and Higinbotham (1976), found that older maize root segments are electrically more conductive than younger roots. Their study was performed on excised root segments. They showed that the outer layer of the root segment (cortex) has very low electrical resistance (~ 50 k Ω) in the radial direction when compared to the axial direction (~ 600

k Ω). By treating cortex and stele as concentric parallel conductors, the reported resistances, when converted into conductivity are of the order $\sigma_{root} \sim 0.05$ S/m. However, the electrical behavior of intact root segments embedded in the soil might be different as compared to excised segments. Another study by Cao et al. (2010) reported that the root electrical resistance could be related to root properties such as surface area, number of lateral roots and root length. Studies on poplar roots show that σ_{bulk} of the soil-root medium may increase or decrease with the increase in root mass density depending on the age of the plant (Al Hagrey, 2007; Zenone et al., 2008). On the other hand, $\sigma_{bulk-soil}$ depends on several factors, the most important being the porosity of the soil, the electrical conductivity of the soil fluid (σ_w), and SWC. In addition, loamy and clayey soils have a surface conductivity that depends on mineral composition, SWC and σ_w (Friedman, 2005).

Literature on root electrical properties (Anderson and Higinbotham, 1976; Cao et al., 2010, 2011; Ginsburg and Laties, 1973; Paglis, 2013) and pedophysical models for soils (Al Hagrey, 2007; Amente et al., 2000; Bhatt and Jain, 2014; Friedman, 2005; Garré et al., 2011; Laloy et al., 2011; Werban et al., 2008; Wunderlich et al., 2013) suggests that if the contrast between σ_{root} and $\sigma_{bulk-soil}$ is large enough, roots could have a measurable impact on ERT inversion results. In addition there are studies that found a correlation between root length/mass density and electrical resistivity obtained from ERT (Amato et al., 2009; Rossi et al., 2011). These studies used destructive methods to determine root length density and root biomass. However, to our knowledge, there are no detailed modeling efforts to investigate the effects of roots on electrical conductivity of the bulk medium when monitoring SWC in cropped fields using the ERT method.

Beyond the impact of the electrical conductivity of root tissues, root-related processes like water uptake, exudation or solute uptake will also affect the electrical properties of the rhizosphere, i.e. the soil zone in close proximity to root segments, thereby affecting the $\sigma_{root} - \sigma_{bulk-soil}$ contrast. Recent ERT experiments on orange orchard fields suggest that ERT results are more sensitive to root water uptake pattern (Vanella et al., 2018) than the presence of resistive lignified roots. While this may be true for orange trees, we need a thorough study to investigate the sensitivity of ERT results on the presence of different types of root that are more electrically conductive than soil. Therefore, to investigate the impacts of roots on ERT derived SWC, we should take into account the root water uptake, soil heterogeneity, root specific electrical property along with root growth.

To validate and quantify the impact of roots on ERT-derived SWC, we propose to simulate a virtual 2D rhizotron experiment equipped with ERT. 2D rhizotrons are thin containers (typically around 1 cm x 50 cm x 50 cm) filled up with a growing substrate in which plant roots develop. They are used in soil-plant interactions study to investigate how change in soil conditions might affect plant growth and uptake (e.g. Bauke et al., 2017). They allow the observation of the root system architecture evolution and sometimes of the substrate water content by light transmission (Garrigues et al., 2006) or neutron tomography (Ahmed et al., 2018). In this study, we choose a 2D rhizotron geometry because it offers simplicity yet elegant environment to understand the impact of roots on ERT derived water content. It also allows a further validation of a numerical model, later with a real experiment where root architecture and water content distributions are measured.

Al Hagrey and Petersen (2011) studied the impact of roots on ERT imaging by using a root growth model (Wilderotter, 2003), however they ignored the inherent heterogeneity of σ_{root} and $\sigma_{bulk-soil}$. To understand the effect of root system connectivity and their impact on SWC on σ_{bulk} , a model where roots are explicitly represented is needed. Explicit root representation using an unstructured finite element mesh has been studied for water and nutrient uptake processes (Tournier et al., 2015; Wilderotter, 2003), but to the best of our knowledge, no such work exists for ERT simulations coupled to a plant-soil water flow model.

The objective of this study is to investigate how a transpiring, growing plant might affect the ERT estimate of SWC. We hypothesize that the σ contrast between the plant root system and the soil surrounding the roots (impacted by root, soil properties, and plant hydraulic boundary conditions) together with the amount of roots will affect the ERT measurements and therefore ERT-derived quantities. In our work, we model the electrical conductivity of the soil-root system in a rhizotron geometry with a fine spatial resolution for the roots using an unstructured mesh for the ERT simulation. The root model includes transient transpiration, root growth and root and soil water redistribution. We choose the maize root system for our study and exclude root exudation and solute uptake processes. We also study anisotropy in the electrical conductivity induced by root growth and the water depletion pattern. An accurate electrical conductivity model of the soil-root system will improve our understanding of the electrical behavior of the soil-root zone and hence will help us in improving the ERT method as a feasible and faster tool to monitor soil moisture in

vegetated land. This study is therefore a first step towards a thorough understanding of the impact of roots on SWC monitoring using the ERT method.

2 Materials and Methods

Our numerical experiment consists of running a combination of highly detailed simulations representing the soil water fluxes in a planted 2-D rhizotron along with an ERT simulation. Root and soil electrical and hydraulic properties were explicitly accounted for and spatially distributed with a high resolution to study how root architecture and water uptake influence the ERT imaging results and the interpretation in terms of SWC. Fig. 2 summarizes the various steps described below in a flowchart.

2.1 Rhizotron/plant water flow model

A two-dimensional root architecture was extracted from light transmission experiments on a real rhizotron with a 21 days old maize species using the root image analyzing tool smartroot (Lobet et al., 2011). The digitized root (see Fig.3) was then used for root water uptake modeling using R-SWMS (Javaux et al., 2008). Since the root growth was monitored every day, ages were easily assigned to each root segment. Root growth was simulated by updating the root system architecture at each time step between the beginning (day 5) and the end (day 22) of the simulation. Cyclic transpiration demand was imposed as top boundary condition for the root system. The daily transpiration was supposed to linearly increase between the root emergence and the end of the study. At day 22, daily transpiration reached 25 cm³ and was measured by weight difference.

The root system is entirely contained in soil box whose length, thickness and depth were 22 cm, 1 cm, and 40 cm respectively (the corresponding reference axes are $-11 < x < 11$ cm, $-0.5 < y < 0.5$ cm, $-40 < z < 0$ cm). In the scenario analysis, we considered both sandy and loamy soil types whose hydraulic properties were supposed to be perfectly represented by Mualem-van Genuchten equations (van Genuchten, 1980). Hydraulic parameters for both soils are given in Table 1.

The initial soil condition was a hydrostatic equilibrium with a saturated soil at the bottom of the rhizotron (corresponding to experimental conditions) and root water uptake was the only source/sink term that allowed the total water content to change. R-SWMS uses the finite element method on a regular uniform grid to solve Richards equation in order to simulate three-dimensional water flow in the soil:

$$\frac{\partial \theta}{\partial t} = \frac{\partial}{\partial x} \left(K \frac{\partial h}{\partial x} \right) + \frac{\partial}{\partial y} \left(K \frac{\partial h}{\partial y} \right) + \frac{\partial}{\partial z} \left(K \frac{\partial (h+z)}{\partial z} \right) - Sink \quad [1]$$

,where θ is the volumetric SWC, h the matrix head, K the isotropic hydraulic conductivity, $Sink$ is a sink term for root water uptake [$\text{cm}^3 \text{ cm}^{-3} \text{ day}^{-1}$], and x, y and z are the spatial coordinates. Experimentally measured maize root hydraulic conductivities were used in the R-SWMS model, in which they are age and type dependent (Couvreur et al., 2012; Doussan et al., 2006). Two-dimensional distributions of roots and of SWC were subsequently transformed into electrical conductivity maps through appropriate bio-pedo electrical relations.

2.2 Electrical properties of plant root tissues and soils

To get insight into maize root electrical properties, we designed specific experiments on intact root segments (Ehosioke et al., 2018). First, we identified and separated the primary and brace roots from maize plants grown in laboratory and were thoroughly washed with demineralized water and dried with absorbent tissue. The electrical resistance of root segments was measured using a digital multimeter and were converted into electrical conductivity (σ_{root}) by approximating the root segment as a cylindrical geometry similar to Cao et al. (2010). The measurement direction of root segments in Cao et al. (2010) is from root apex towards root collar while it is opposite in the case of our experiment. We studied intact root segments as compared to excised root segments in the studies of Cao et al. (2010) or Anderson and Higinbotham (1976) and investigated both primary and brace roots in the experiments. We examined variations of σ_{root} with respect to the segment distance from the root collar and root cross-sectional area with a segment length of 4 cm. Conductivity gel (*Rodisonic*, from Pannoc Nv/SA Belgium) was used to improve the electrical contact between root segments and measuring electrodes. However, in the simulation model, only the variations of σ_{root} as a function of segment distance from the root collar is used. The digital maize roots in our simulation are around three weeks old while the brace roots develop only after several weeks in a real maize plant; hence, the brace root data are not included in our model.

To compute soil electrical properties, we used Archie's law (Archie, 1942) with an additional term for surface conductivity of the solid phase $\sigma_{surface}$, which is assumed to act in parallel (Waxman and Smits, 1968). The relation between soil water content θ and σ_{soil} for unsaturated soil is given by Eq. 2, where Archie's fitting parameters (m and d) vary for different types of soil (Friedman, 2005):

$$\sigma_{bulk-soil} = \sigma_w n^m S^d + S^{d-1} \sigma_{surface}, \quad [2]$$

where, S is the degree of water saturation ($S = \frac{\theta}{n}$), n the porosity of soil (assumed to be equal to saturated water content: θ_s), $\sigma_{bulk-soil}$ the bulk electrical conductivity of the soil medium without considering roots (more specifically, $\sigma_{bulk-loam}$ for loam and $\sigma_{bulk-sand}$ for sand), σ_w the conductivity of soil fluid phase, $\sigma_{surface}$ is the surface electrical conductivity of the solid phase of the soil. Sand typically has very low surface conductivity ($\sim 10^{-5} S/m$) while for loam, we assume $\sigma_{surface}$ to be 0.015 S/m (Brovelli and Cassiani, 2011). For Archie's fitting parameters, we use the typical values $d = 2$ and $m = 1.3$ (e.g. Werban et al., 2008). $\sigma_{bulk-soil}$, in the rhizotron also depends on the electrical conductivity of the nutrient solution (σ_w) in the rhizotron used to grow plants. Measurements from suction cups indicate that σ_w varies between 0.06 to 0.2 S/m (Jougnot et al., 2012). We assume σ_w to be 0.2 S/m and choose n as 0.35 (sand) and 0.435 (loam), respectively, for calculating and comparing different pedophysical models. In the following sections, we will refer $\sigma_{bulk-soil}$ as the soil bulk electrical conductivity (with $\sigma_{bulk-loam}$ and $\sigma_{bulk-sand}$ to specify soil type) when no roots are present and σ_{bulk} will be used for studies or dataset where both roots and soil are present.

2.3 Electrical modeling in EIDORS

The ERT forward problem seeks apparent conductivity or voltage data by solving the Poisson's equation with appropriate boundary conditions with a known electrical conductivity distribution. In ERT inverse problems, we aim at reconstructing an estimate of the electrical conductivity distribution within the soil-root domain from apparent conductivity or voltage measurements at its boundary or at some discrete locations within the computational domain. The inverse problem finds an approximate σ -distribution that minimizes the data misfit between the virtual measurements and the model predictions in a least-square sense in addition to a regularization term. We use the finite-element based software EIDORS (Adler and Lionheart, 2006) to solve the forward and inverse problems as it offers flexibility in using different meshing software such as NETGEN (Schöberl, 1997) and gmsh (Geuzaine and Remacle, 2009). The integration of such meshing software allows creating complex finite-element models for electrical conduction in a soil-root medium. The electrical conduction model for the rhizotron is in purely 2-D (x-z plane, $y=0$). A point electrode model (Hanke et al., 2011) with a total number of 50 electrodes and a dipole-dipole measurement

scheme is used to compute the forward response. All the electrodes are located at the boundary of the computational domain with a similar set-up as in Weigand and Kemna (2017). Three different finite-element meshes are used (Fig. 4). To simulate the ERT data set, the root growth simulation model mesh (SMDL), with an explicit representation of the root architecture is used. The ERT forward model mesh (FMDL), which does not contain the root architectural information, is used to compute the data misfit in the ERT inversion, and the ERT inverse mesh, a comparatively coarse mesh is used to compute the Jacobian in the ERT reconstruction. In the SMDL, either a σ_{root} or $\sigma_{bulk-soil}(\theta)$ value is assigned to each element. The maize primary roots in our simulation have a mean thickness (~ 0.05 cm) which is small compared to the dimensions of rhizotron (20x40 cm), requiring a very high spatial resolution for roots in the SMDL. The total root length per unit volume in RSWMS simulation was 0.06, 0.22, 0.66, 1.1, and 1.61 cm/cm³ at day 5,10,15,18 and 22, respectively. In the typical field, mature root density reaches values of 1cm/cm³, especially in the top soil (Gao et al., 2010).

To generate a root resolved mesh with high spatial resolution, first we created the binary images of root architectures at various ages (day 5, 7, 10, 12, 15, 18, 22, see Fig. 3). In these binary images, we removed extremely fine root hairs and root branches that were below 0.01 cm in thickness, assuming that such roots have negligible effect on the electric potential distribution. The simplified root image represent root branches with a mean diameter of 0.05 cm. Second, we convert binary images into a spline functions that trace the boundary of the root surfaces (red lines in Fig. 4 b) using the boundary tracing function “bwboundaries” in MATLAB. The spline function representing the root shape was converted into finite element mesh using gmsh software. The root architecture mesh created in this manner possesses superior quality in terms of aspect ratio of elements and is computationally efficient. We then solved the electrical forward problem for the generated σ -map yielding virtual ERT data, which is subsequently inverted using EIDORS. The Gauss-Newton (GN) one-step inversion algorithm used in this study requires ERT forward data to be taken on two different conductivity distributions, so that the change in conductivity can be estimated. To do so, first we generate a forward data set (d_1) for a homogeneous σ -distribution as the first medium ($\sigma_1 = 1$ S/m). Then the second forward data d_2 is computed on a medium σ_2 , which is the sum of soil root electrical conductivity and σ_1 (that is, $\sigma_2 = \sigma_1 + \sigma_{bulk}$). Using the change in measurement ($\delta d = d_2 - d_1$), change in conductivity ($\delta \sigma = \sigma_2 - \sigma_1 \sim \sigma_{bulk}$) is estimated by GN one-step algorithm (Adler et al., 2007). The high value chosen for σ_1 (1 S/m)

make sure that the change in conductivity and change in measurement can be linearly related as required by GN one-step algorithm. The maximum conductivity in sand medium (~ 0.04) and in loam medium (~ 0.07) is within 10 %, when compared to σ_1 ensuring linearity between $\delta\sigma$ and δd . Finally, the inversion is regularized using a Laplacian matrix (smoothing constraint). To simulate noise in data, δd is added with 1% random noise proportional to each measurement. The FMDL mesh is used to compute the ERT data (δd) and the data misfit while the inverse mesh is used for the inversion.

2.4 Computing average and effective electrical properties

In the following sentences, the average electrical conductivity denoted by $\langle\sigma_{bulk}\rangle$ is defined as the spatially averaged electrical conductivity data from the SMDL mesh while the effective electrical conductivity denoted by σ_{bulk} is defined as the electrical conductivity computed using simulated plate electrodes on the SMDL mesh.

To get an insight on how a rooted soil might differ from bare soil pedophysical model (Eq. 2), we compare bulk electrical conductivity of soil-root medium, at two different scales: 2x2 cm and 20 x 40 cm.

At smaller scale, the block-wise averaged data, denoted by $\langle\sigma_{bulk}\rangle$ and $\langle\theta\rangle$ for electrical conductivity and water content respectively , are computed from averaging the corresponding data in the simulation model finite element mesh with an averaging block size of 2cm x 2cm (see Fig. 7a). Averaging in each block is done by taking the arithmetic and the harmonic averages of conductivity data of all finite elements within each averaging block to get $\langle\sigma_{bulk}\rangle$. The arithmetic averages assumes that the soil-root elements in each averaging block are connected in series while the harmonic mean assumes the elements to be in parallel. For $\langle\theta\rangle$, we computed only the arithmetic mean. In reality we expect, the real $\langle\sigma_{bulk}\rangle$ to be in between the arithmetic and harmonic averages, depending on the main angular orientation of the roots segments. The relation between the collection of averaged data points at every averaging block and at all time (day 5 to , i.e. $\langle\theta\rangle$ vs $\langle\sigma_{bulk}\rangle$, will then approximately mimic the impact of roots at a block-scale on σ_{bulk} , when compared to the Archie's law applied in soils only (Eq.2).

At larger scale (rhizotron scale, i.e. 20cm x 40 cm), simple mean of arithmetic and harmonic averages over whole domain may not exactly represent bulk property, since we need to account for the complex structural variations of electrical conductivity distributions and heterogeneity in soil

electrical property. Hence, to compute σ_{bulk} , at the scale of the rhizotron, we solve the Poisson's equation between two plate electrodes at the boundaries with root included (a root segment has its own electrical conductivity) and without root. The computation is repeated for two directions: in horizontal (σ_{bulkX}) and vertical direction (σ_{bulkZ}). We included in our simulations, the plate electrodes that cover the entire left and right walls of the rhizotron as well as top and bottom wall of rhizotron and the ratio of injected current to measured voltage in these electrodes with the geometric factor considerations gives σ_{bulkZ} and σ_{bulkX} .

3 Results

3.1 Electrical measurements on Maize root segments

Figure 5a shows the experimental data of σ_{root} as a function of root age for Maize. We observe a gradual increase in σ_{root} of intact maize root segments, as the segment distance from root collar increased (Fig. 5a). The trend is different in primary and brace roots, where the brace root conductivity increases much more rapidly with increasing distance of the segment from the root collar compared to primary root segments. The σ_{root} also varies with respect to root cross-sectional area. Our measurements indicate that thinner roots have higher σ_{root} compared to thicker roots (Fig. 5b). This could be due to higher water content of younger roots. Since we measured intact root segments, the surface electrical conductivity of endodermis and contact resistance of stele and cortex layers of the root are accounted for in the measurements. The thicker outer layer (cortex) of the root is electrically more insulating than water rich younger roots or inner part (stele) as seen in early studies of Anderson et al. (1976). However, our measurements represent the combined resistivity of cortex and stele in an intact form. Age dependent electrical conductivity variations within a given species were earlier studied in poplar roots (Zenone et al., 2008). Fig. 5a shows that within the same species, in addition to age, different types of roots (brace and ground roots) can have different electrical properties. However, in the modeling work, we do not consider the development of brace roots as the simulated root system in the model is relatively young (3-weeks old). The blue-curve of Fig. 5a represents the data incorporated in our simulations: $0.0154 < \sigma_{root} < 0.03$ [S/m].

3.2 Virtual root simulation

Simulations show that the relative SWC distribution patterns depend on the soil type (Figs. 6 a, b). After 22 days, the depletion is higher in the sand rhizotron as θ_s is lower. In the loam, the soil is

wetter and the difference between saturation of the rooted and unrooted parts of the soil is much more contrasted.

When translated into electrical conductivity maps including the root electrical properties, we see different trends for sand and loam. For sand, we notice that σ_{root} is always larger than $\sigma_{bulk-sand}$ and the difference between σ_{root} and $\sigma_{bulk-sand}$ is always positive (Fig. 6c). For loam, however, we see that different regions where $\{\sigma_{root}, \sigma_{bulk-loam}\}$, contrast changes with time (Fig. 6d). At initial time, $\sigma_{bulk-loam}$ is larger than σ_{root} but at day 18, we see different regions, where the difference between σ_{root} and $\sigma_{bulk-loam}$ is either positive, negative or close to zero. Such contrast does not manifest in sand. At day 22, in the upper portion of rhizotron, σ_{root} is greater than $\sigma_{bulk-loam}$ whereas in the lower portion of rhizotron, the roots are masked by $\sigma_{bulk-loam}$ (see Fig. 6d). In real scenarios, i.e in any soil-root system, there potentially exist three regions, where the difference between σ_{root} and $\sigma_{bulk-soil}$ is either positive, negative or close to zero, assuming that the salinity of the soil solution doesn't change significantly around roots. In our simulations, we observe that at low SWC, the mean of σ_{root} is greater than the mean of $\sigma_{bulk-loam}$ and at high water content, the mean of σ_{root} is lower than the mean of $\sigma_{bulk-loam}$, while in sand, the mean of σ_{root} is nearly same as the mean of $\sigma_{bulk-sand}$ (Fig. 6e). Since electric current flow depends on the gradient of σ -distribution, the effect of roots in ERT experiments will be greater where there is higher $\{\sigma_{root}, \sigma_{bulk-soil}\}$ contrasts and most importantly, it is time dependent (Fig. 6e). In addition, the density of roots plays a role in terms of $\{\sigma_{root}, \sigma_{bulk-soil}\}$ contrasts, for instance at day 22, the upper part of the root system is more conductive than $\sigma_{bulk-loam}$ in the upper part of the rhizotron and also reflects higher root volume than at initial times. Therefore, at later times (Fig. 6d, day 22), the ERT estimate of water content in the upper region could be misleading due to a stronger root influence on σ_{bulk} .

3.3 Bulk electrical properties

The block wise averaged electrical conductivity data points lie along the Archie's curve for low root density regions and deviates significantly from the Archie's curve for high root density regions (Figs. 7 b and d). In sand, we see more difference between arithmetic and harmonic mean with harmonic mean staying closer to the original pedophysical curve than the arithmetic one (Fig. 7b). In loam, however, there is no big difference between arithmetic and harmonic block wise averaged data and both of them change the curvature of the pedophysical relation (Fig. 7d). As expected, when root density is high, the $\langle\theta\rangle$ vs $\langle\sigma_{bulk}\rangle$ plot significantly deviates from Eq. 2 and always

overestimates $\sigma_{bulk-sand}$, whereas areas with very low to zero root density lie along $\sigma_{bulk-soil}(\theta)$ curve (blue dots on $\sigma_{bulk-soil}(\theta)$ curve for $\theta > 0.2$ in Fig. 7b and $\theta > 0.3$ in Fig. 7d). In loam, the $\langle\theta\rangle$ vs $\langle\sigma_{bulk}\rangle$ points are scattered around the petrophysical relationship with a tendency of both overestimating $\sigma_{bulk-loam}$ for $\theta < 0.2$ and underestimating $\sigma_{bulk-loam}$ for $\theta > 0.2$ in the root dense region. This illustrates how roots might affect the relationship between SWC and σ_{bulk} .

At the rhizotron scale, the effective bulk property shows significant anisotropic affect in sand (notice the difference between σ_{bulkX} and σ_{bulkZ} in Fig. 7 (d and g)). We expect that the dry sand act as a barrier to the electrical current flow, thereby decreasing the σ_{bulk} . The vertical direction has more pronounced anisotropy, when compared to horizontal direction ($\sigma_{bulkX} > \sigma_{bulkZ}$), as we see less deviation of σ_{bulkX} from Archie's law when compared to σ_{bulkZ} . This is due to horizontal layering that develops in the electrical conductivity distribution due to root water uptake, which thereby affects current more in vertical direction than in horizontal direction. For loam medium, the anisotropic effect is less when compared to sand. We see from the effective bulk properties that the original pedophysical relation (Archie's law) would rather under-estimate the water content in loam where as it would over-estimate in sand (Fig.7 c and e). Computed σ_{bulkX} and σ_{bulkZ} data points lie below $\sigma_{bulk-soil}(\theta)$ in sand medium whereas above in the loam medium. The rhizotron scale, bulk electrical conductivity deviates from Archie's law quite differently when compared to the averaged data at smaller scale (Fig.7 b, c, e, and f). This can be understood as the impact of soil heterogeneity playing a bigger role in influencing the bulk property at large scale whereas at centimeter-scale (2cm x 2cm), the root density plays a major role in the deviating the bulk property from bare soil pedophysical relation (Eq.[2]).

Table 2 gives the computed anisotropy factor, $AF = \sigma_{bulkX}/\sigma_{bulkZ}$ for cases with and without roots. As we can see from the table, the main anisotropic affect is due to soil heterogeneity and not the root themselves.

3.4 ERT Inversion result

The GN one-step inversion was performed on the virtual measurement data set from the forward conductivity distribution with root system included (Figs. 8 a, d) and without considering the root system. The inversion of ERT data without considering root segments were realized by inverting the voltage data virtually collected on the soil water content map only (see Fig. 6 a,b), without considering the root electrical properties. Figures 8b and 8e shows the ERT inversion with root system included sand and loam medium, respectively. As we can see, the inversion works well in

recovering most of the important features of soil water depletion, but sometimes we can observe contamination due to the presence of roots (for example day 18 and 22 in Fig. 8b). Note that for sand the presence of roots increased the electrical conductivity while for loam it decreased the electrical conductivity.

Figures 8c and 8f represents the difference in the inversion results of virtual data from forward conductivity distributions with and without root systems. The inversion result with roots is showed in Figs 8 (b and e) but the inversion results without considering the root system are not shown here. This difference maps in Figs. 8c and 8f represents the error that could occur by ignoring the presence of the roots in the forward model on the ERT inverted σ -distributions. In sand, the error can be as low as 2% when the roots are small and can reach up to 15% when soil becomes dry and roots occupy the whole rhizotron. This error manifests as wrong water content estimate, if we use bare soil pedophysical function such as Archie's law to interpret ERT result (see flowchart in Fig.2).

By comparing Figs. 8(a,b,c) and 8 (d,e,f), we can immediately see that in loam, the soil is more conductive than root at most time. Roots are like low conductive wires in the loam medium surrounded by highly conductive soil. Since $\sigma_{bulk-loam}$ dominates the effective properties, the impact of roots is also lower in loam compared to that of sand. At later time (Fig. 8d, day 22), as root water uptake becomes significant, the contrast between $\sigma_{bulk-loam}$ and σ_{root} reduces making roots indistinguishable from soil. Figures 8c and 8f indicate that the error in the estimation of the conductivity /water content increases with ongoing root growth. While the error pattern is monotonic in sand increasing with root growth, in loam we see different regions of high and low error depending on soil-root contrast. These errors in σ -estimate manifest in the SWC estimated from Archie's law. We denote here, the volumetric average of water content from RSWMS simulation by: θ_1 , volumetric average of water content from ERT inverted σ -map without the root electrical properties in the ERT forward data by: θ_2 , and volumetric average of water content from ERT inverted σ -map with the root electrical properties included in the ERT forward data by: θ_3 . We show θ_1 , θ_2 and θ_3 as a function of time in Figure 9 (a, d). The difference between θ_1 and θ_2 is the error induced due ERT inversion procedure alone while the difference between θ_1 and θ_3 is the error induced due to ERT method as well as the root segments. In Figure 9 (b,c,e,f), we show that these errors in absolute and relative terms are more pronounced when the root system is large. When the root is young (age <10 days), the absolute error between θ_1 and θ_2 is same as the

absolute error between θ_1 and θ_3 indicating that root segments has no significant impact in water content estimates (Fig. 9b and e).

4 Discussions

Soil-root water flow modeling together with root electrical measurements reveals that soil-root electrical conductivity contrasts changes over time (Fig. 6) as a function of soil type and root water uptake. This soil-root σ contrast could impose error in water content estimates. To characterize the specific impact of roots in ERT monitored water content estimates, we need the knowledge of σ contrast between root and soil as a function of space and time. Estimating this contrast between root and soil, however, is not so straightforward and difficult in a real experiment, as they are root type, root age, root radius, soil type and water content dependent.

Both averaging and effective properties reveal that rooted soil deviates from pedophysical relation of bare soil (Fig.7). This is consistent with the experimental observation made by Michot et al., (2016), where they found that bare-soil pedophysical relation is inadequate to explain $\sigma_{bulk}(\theta)$ in the rooted zone. Further upscaling the electrical properties derived from centimeter scale (root segment) to decimeter scale (rhizotron) to field scale (~100 meter) is very important to develop a proper pedophysical relation that completely eliminates the root impact in the water content estimate. We considered a very limited range in $\sigma_{root} - \sigma_{bulk-soil}$ variability in the model. In reality, the range of variations in $\sigma_{root} - \sigma_{bulk-soil}$ could differ depending on the type of roots and the value of σ_w (Fig.1).

Modeling results indicate an anisotropy factor of around six for fully mature maize root systems. This is mostly due to water content distribution pattern induced by root water uptake. At rhizotron scale, anisotropy is stronger in sand, when compared to loam, and increases non-linearly with root growth (Table 2). Although the maize simulations in this study indicates that water content is the dominant factor affecting bulk electrical conductivity, other factors do play a role including the root connectivity that induces electrical anisotropy. Since our model indicates a non-negligible anisotropy factor in the electrical conductivity, this information could be used to phenotype different root systems. A prior knowledge of time dependent electrical conductivity contrasts between soil and root including electrical anisotropy, for a given crop, can definitely help in designing optimized ERT injection scheme for the future field experiments. ERT injection scheme

should consider exploiting anisotropy to retrieve better information, for example, by having an injection scheme that maximizes the sensitivity in the region of anisotropy. However, this would also require an anisotropic ERT inversion scheme (Pain et al., 2003; Wiese et al., 2015).

We must consider some real world limitations, if the process-based model described here is extended to a real experiment. For example, in the agricultural fields as well as in 2D rhizotron, air filled cracks can manifest in the soil, potentially influencing ERT measurements which our model does not account for. For future validation of modeling results presented here in a real experiment, limitations in ERT such as bad electrode contact and other artifacts such as soil cracks can be combatted with repeated measurements and adjustments during the course of experiment ,which is simpler to implement in a Rhizotron experiment than in the real field (Huck and Taylor, 1982).

Our model did not consider rhizosphere processes such as root exudation, which could also affect the water content estimates. We assumed, in the model, that the roots absorb solute in proportion to the water uptake, so that there is no accumulation of salts near the roots as observed by Beff et al (2013), but this assumption might not always be valid. Solute gradients, if it were to occur, near the roots could drastically change the forward conductivity map thereby affecting the water content estimate due to salinity change around root will be in-between σ_{root} and σ_w .

In reality, soil-root systems are three-dimensional structures and two-dimensional rhizotron approximations may overestimate the impact of root on ERT estimated water content as compared to real soil-root environments (e.g. cropped fields). However, the proposed process-based methodology should be extended to consider 3D effects in the future work.

Finally, we also ignored the anisotropy of σ inside the root structure (stele-cortex variations), which may have a considerable effect on ERT measurements. Such structural variations may induce even higher degree of anisotropy in the electrical conductivity. Our next step will be the validation of our findings in real experiments.

5. Conclusions

We used a process-based model to simulate the electrical conductivity distribution in a 2D rhizotron. The roots were explicitly represented and root water uptake was simulated using a mechanistic water flow model in soil and roots. The impact of soil type and change of water content were represented with a petrophysical relation. In addition, the root conductivity map was explicitly

accounted for, based on measurements made on maize root segments indicating that σ_{root} is a function of distance from the root collar and root type (primary and brace roots). We incorporated the distance variations of primary roots into our model based on a polynomial fit. We then performed virtual ERT inversions on generated σ -distribution to investigate impact of roots. The modeling work described here is one of the first attempts taken to understand root impact on ERT data.

Analysis on σ -distributions generated by simulated root water uptake and root system architecture showed an impact on the apparent petrophysical relations. This effect was further increased by the root system growth (i.e., function of the root length density) and by the contrast between soil and root electrical resistivities. The impact of soil water depletion was always visible on the averaged electrical conductivity but was sometimes counter balanced by root growth. This might lead to non-negligible errors in retrieving the soil water content (up to 200% relative error). Even though the effect of roots at rhizotron scale is not evident in the forward bulk property analysis of electrical conductivity data, it is evident in ERT inversion result. This indicates the importance of incorporating the effect of roots in the pedophysical model. ERT inversions on simulated data recover the overall trend of decrease in total water content due to root water uptake, with an error (by ignoring roots in forward data) in inverted σ ranging from 5 to 15 %. For maize roots, the water uptake process dominates the σ -distribution of the soil-root system as reconstructed with ERT.

Further work will to come this study could be to correct field scale ERT dataset from the impact of roots. To do this, we could collect a database of root electrical conductivity for different cropped species and then with the help of root system architecture modeling software such as Crootbox (Schnepf et al., 2017), the study presented here could be extended to different species. We could then integrate these information's (root electrical conductivity and root system architecture) into the coupled soil-root electrical model described here to study the impact of roots under different scenarios and can be compared with real field experiments. Such a study would also shed light on whether ERT data has information on root phenotyping and if so, what can be done to maximize the information. In addition, this modeling work could also benefit the development of bio-pedophysical relationship in the rooted soil that takes root morphological features and its electrical properties into account. Such bio-pedophysical models will minimize the error in SWC estimates in cropped field from ERT method.

References

- Adler, A. and Lionheart, W. R. B.: Uses and abuses of EIDORS: an extensible software base for EIT, *Physiological Measurement*, 27(5), S25, 2006.
- Adler, A., Dai, T. and Lionheart, W. R. B.: Temporal image reconstruction in electrical impedance tomography, *Physiol. Meas.*, 28(7), S1, doi:10.1088/0967-3334/28/7/S01, 2007.
- Ahmed, M. A., Zarebanadkouki, M., Meunier, F., Javaux, M., Kaestner, A. and Carminati, A.: Root type matters: measurement of water uptake by seminal, crown, and lateral roots in maize, *J Exp Bot*, 69(5), 1199–1206, doi:10.1093/jxb/erx439, 2018.
- Al Hagrey, S. A.: Geophysical imaging of root-zone, trunk, and moisture heterogeneity, *Journal of Experimental Botany*, 58(4), 839–854, doi:10.1093/jxb/erl237, 2007.
- Al Hagrey, S. A. and Petersen, T.: Numerical and experimental mapping of small root zones using optimized surface and borehole resistivity tomography, *Geophysics*, 76(2), G25–G35, doi:10.1190/1.3545067, 2011.
- Amato, M., Bitella, G., Rossi, R., Gómez, J. A., Lovelli, S. and Gomes, J. J. F.: Multi-electrode 3D resistivity imaging of alfalfa root zone, *European Journal of Agronomy*, 31(4), 213–222, doi:10.1016/j.eja.2009.08.005, 2009.
- Amente, G., Baker, J. M. and Reece, C. F.: Estimation of Soil Solution Electrical Conductivity from Bulk Soil Electrical Conductivity in Sandy Soils, *Soil Science Society of America Journal*, 64(6), 1931–1939, doi:10.2136/sssaj2000.6461931x, 2000.
- Anderson, W. P. and Higinbotham, N.: Electrical Resistances of Corn Root Segments, *Plant Physiology*, 57(2), 137–141, 1976.
- Archie, G. E.: The Electrical Resistivity Log as an Aid in Determining Some Reservoir Characteristics, *SPE-942054-G*, doi:10.2118/942054-G, 1942.
- Bauke, S. L., Landl, M., Koch, M., Hofmann, D., Nagel, K. A., Siebers, N., Schnepf, A. and Amelung, W.: Macropore effects on phosphorus acquisition by wheat roots – a rhizotron study, *Plant Soil*, 416(1), 67–82, doi:10.1007/s11104-017-3194-0, 2017.
- Beff, L., Günther, T., Vandoorne, B., Couvreur, V. and Javaux, M.: Three-dimensional monitoring of soil water content in a maize field using Electrical Resistivity Tomography, *Hydrol. Earth Syst. Sci.*, 17(2), 595–609, doi:10.5194/hess-17-595-2013, 2013.
- Bhatt, S. and Jain, P. K.: Correlation between electrical resistivity and water content of sand – a statistical approach, *Am. Int. J. of Res. in Sci., Tech., Eng. & Math.*, 6(2), 115–121, 2014.
- Brillante, L., Bois, B., Lévêque, J. and Mathieu, O.: Variations in soil-water use by grapevine according to plant water status and soil physical-chemical characteristics-A 3D spatio-temporal analysis, *European Journal of Agronomy*, 77, 122–135, doi:10.1016/j.eja.2016.04.004, 2016.
- Brovelli, A. and Cassiani, G.: Combined estimation of effective electrical conductivity and permittivity for soil monitoring, *Water Resour. Res.*, 47(8), W08510, doi:10.1029/2011WR010487, 2011.

530 Cao, Y., Repo, T., Silvennoinen, R., Lehto, T. and Pelkonen, P.: An appraisal of the electrical resistance
531 method for assessing root surface area, *Journal of Experimental Botany*, 61(9), 2491–2497,
532 doi:10.1093/jxb/erq078, 2010.

533 Cao, Y., Repo, T., Silvennoinen, R., Lehto, T. and Pelkonen, P.: Analysis of the willow root system by
534 electrical impedance spectroscopy, *Journal of Experimental Botany*, 62(1), 351–358,
535 doi:10.1093/jxb/erq276, 2011.

536 Couvreur, V., Vanderborght, J. and Javaux, M.: A simple three-dimensional macroscopic root water
537 uptake model based on the hydraulic architecture approach, *Hydrol. Earth Syst. Sci.*, 16(8), 2957–2971,
538 doi:10.5194/hess-16-2957-2012, 2012.

539 De Carlo, L., Battilani, A., Solimando, D., Battilani, A., Lo Porto, A. and Caputo, M. C.: Monitoring different
540 irrigation strategies using surface ERT, pp. 71–75. [online] Available from:
541 [https://www.scopus.com/inward/record.uri?eid=2-s2.0-](https://www.scopus.com/inward/record.uri?eid=2-s2.0-84957960460&partnerID=40&md5=d5a2e82335284345a7097045eaaad93b)
542 [84957960460&partnerID=40&md5=d5a2e82335284345a7097045eaaad93b](https://www.scopus.com/inward/record.uri?eid=2-s2.0-84957960460&partnerID=40&md5=d5a2e82335284345a7097045eaaad93b), 2015.

543 de Dorlodot, S., Forster, B., Pagès, L., Price, A., Tuberosa, R. and Draye, X.: Root system architecture:
544 opportunities and constraints for genetic improvement of crops, *Trends in Plant Science*, 12(10), 474–
545 481, doi:10.1016/j.tplants.2007.08.012, 2007.

546 Doussan, C., Pierret, A., Garrigues, E. and Pagès, L.: Water Uptake by Plant Roots: II – Modelling of Water
547 Transfer in the Soil Root-system with Explicit Account of Flow within the Root System – Comparison with
548 Experiments, *Plant Soil*, 283(1–2), 99–117, doi:10.1007/s11104-004-7904-z, 2006.

549 Ehosioko, S., Sarah Garré, Kremer, T., Rao, S., Kemna, A., Huisman, J., Zimmermann, E., Javaux, M. and
550 Nguyen, F.: A New Method For Characterizing The Complex Electrical Properties of Root Segments,
551 conference paper, 10th Symposium of the International Society of Root Research, July 2018, Israel.
552 [online] Available from:
553 <https://events.eventact.com/ProgramView2/Agenda/Lecture?id=172928&code=3547344>, 2018.

554 Friedman, S. P.: Soil properties influencing apparent electrical conductivity: a review, *Computers and*
555 *Electronics in Agriculture*, 46(1–3), 45–70, doi:10.1016/j.compag.2004.11.001, 2005.

556 Gao, Y., Duan, A., Qiu, X., Liu, Z., Sun, J., Zhang, J. and Wang, H.: Distribution of roots and root length
557 density in a maize/soybean strip intercropping system, *Agricultural Water Management*, 98(1), 199–212,
558 doi:10.1016/j.agwat.2010.08.021, 2010.

559 Garré, S., Javaux, M., Vanderborght, J., Pagès, L. and Vereecken, H.: Three-Dimensional Electrical
560 Resistivity Tomography to Monitor Root Zone Water Dynamics, *Vadose Zone Journal*, 10(1), 412–424,
561 doi:10.2136/vzj2010.0079, 2011.

562 Garré, S., Coteur, I., Wongleecharoen, C., Kongkaew, T., Diels, J. and Vanderborght, J.: Noninvasive
563 Monitoring of Soil Water Dynamics in Mixed Cropping Systems: A Case Study in Ratchaburi Province,
564 Thailand, *Vadose Zone Journal*, 12(2), doi:10.2136/vzj2012.0129, 2013.

565 Garrigues, E., Doussan, C. and Pierret, A.: Water Uptake by Plant Roots: I – Formation and Propagation of
566 a Water Extraction Front in Mature Root Systems as Evidenced by 2D Light Transmission Imaging, *Plant*
567 *Soil*, 283(1), 83, doi:10.1007/s11104-004-7903-0, 2006.

568 van Genuchten, M. T.: CLOSED-FORM EQUATION FOR PREDICTING THE HYDRAULIC CONDUCTIVITY OF
569 UNSATURATED SOILS., *Soil Science Society of America Journal*, 44(5), 892–898, 1980.

570 Geuzaine, C. and Remacle, J.-F.: Gmsh: A 3-D finite element mesh generator with built-in pre- and post-
571 processing facilities, *International Journal for Numerical Methods in Engineering*, 79(11), 1309–1331,
572 doi:10.1002/nme.2579, 2009.

573 Ginsburg, H. and Laties, G. G.: Longitudinal electrical resistance of maize roots, *Journal of Experimental*
574 *Botany*, 24(6), 1035–1040, doi:10.1093/jxb/24.6.1035, 1973.

575 Hanke, M., Harrach, B. and Hyvönen, N.: Justification of point electrode models in electrical impedance
576 tomography, *Math. Models Methods Appl. Sci.*, 21(06), 1395–1413, doi:10.1142/S0218202511005362,
577 2011.

578 Huck, M. G. and Taylor, H. M.: The Rhizotron as a Tool for Root Research, in *Advances in Agronomy*, vol.
579 35, edited by N. C. Brady, pp. 1–35, Academic Press., 1982.

580 Javaux, M., Schröder, T., Vanderborght, J. and Vereecken, H.: Use of a three-dimensional detailed
581 modeling approach for predicting root water uptake, *Vadose Zone Journal*, 7(3), 1079–1088,
582 doi:10.2136/vzj2007.0115, 2008.

583 Jougnot, D., Linde, N., Revil, A. and Doussan, C.: Derivation of soil-specific streaming potential electrical
584 parameters from hydrodynamic characteristics of partially saturated soils, *Vadose Zone Journal*, 11(1), 0,
585 doi:10.2136/vzj2011.0086, 2012.

586 Laloy, E., Javaux, M., Vanclooster, M., Roisin, C. and Bielders, C. L.: Electrical Resistivity in a Loamy Soil:
587 Identification of the Appropriate Pedo-Electrical Model, *Vadose Zone Journal*, 10(3), 1023–1033,
588 doi:10.2136/vzj2010.0095, 2011.

589 Lobet, G., Pagès, L. and Draye, X.: A Novel Image-Analysis Toolbox Enabling Quantitative Analysis of Root
590 System Architecture, *Plant Physiol.*, 157(1), 29–39, doi:10.1104/pp.111.179895, 2011.

591 Michot, D., Benderitter, Y., Dorigny, A., Nicoullaud, B., King, D. and Tabbagh, A.: Spatial and temporal
592 monitoring of soil water content with an irrigated corn crop cover using surface electrical resistivity
593 tomography, *Water Resources Research*, 39(5), SBH141–SBH1420, 2003.

594 Michot, D., Thomas, Z. and Adam, I.: Nonstationarity of the electrical resistivity and soil moisture
595 relationship in a heterogeneous soil system: a case study, *SOIL*, 2(2), 241–255, doi:10.5194/soil-2-241-
596 2016, 2016.

597 Paglis, C. M.: Application of Electrical Resistivity Tomography for Detecting Root Biomass in Coffee Trees,
598 *International Journal of Geophysics*, doi:10.1155/2013/383261, 2013.

599 Pain, C. C., Herwanger, J. V., Saunders, J. H., Worthington, M. H. and Oliveira, C. R. E. de: Anisotropic
600 resistivity inversion, *Inverse Problems*, 19(5), 1081, 2003.

601 Rossi, R., Amato, M., Bitella, G., Bochicchio, R., Ferreira Gomes, J. J., Lovelli, S., Martorella, E. and Favale,
602 P.: Electrical resistivity tomography as a non-destructive method for mapping root biomass in an
603 orchard, *European Journal of Soil Science*, 62(2), 206–215, doi:10.1111/j.1365-2389.2010.01329.x, 2011.

604 Schnepf, A., Leitner, D., Landl, M., Lobet, G., Mai, T. H., Morandage, S., Sheng, C., Zoerner, M.,
 605 Vanderborght, J. and Vereecken, H.: CRootBox: A Structural-Functional Modelling Framework For Root
 606 Systems, bioRxiv, 139980, doi:10.1101/139980, 2017.

607 Schöberl, J.: An advancing front 2D/3D-mesh generator based on abstract rules, Computing and
 608 Visualization in Science, 1(1), 41–52, doi:10.1007/s007910050004, 1997.

609 Srayeddin, I. and Doussan, C.: Estimation of the spatial variability of root water uptake of maize and
 610 sorghum at the field scale by electrical resistivity tomography, Plant Soil, 319(1–2), 185–207,
 611 doi:10.1007/s11104-008-9860-5, 2009.

612 Tournier, P.-H., Hecht, F. and Comte, M.: Finite Element Model of Soil Water and Nutrient Transport with
 613 Root Uptake: Explicit Geometry and Unstructured Adaptive Meshing, Transport in Porous Media, 106(2),
 614 487–504, doi:10.1007/s11242-014-0411-7, 2015.

615 Vanella, D., Cassiani, G., Busato, L., Boaga, J., Barbagallo, S., Binley, A. and Consoli, S.: Use of small scale
 616 electrical resistivity tomography to identify soil-root interactions during deficit irrigation, Journal of
 617 Hydrology, 556, 310–324, doi:10.1016/j.jhydrol.2017.11.025, 2018.

618 Waxman, M. H. and Smits, L. J. M.: Electrical Conductivities in Oil-Bearing Shaly Sands, SPE-1863-A,
 619 doi:10.2118/1863-A, 1968.

620 Werban, U., Al Hagrey, S. A. and Rabbel, W.: Monitoring of root-zone water content in the laboratory by
 621 2D geoelectrical tomography, Journal of Plant Nutrition and Soil Science, 171(6), 927–935,
 622 doi:10.1002/jpln.200700145, 2008.

623 Whalley, W. R., Binley, A., Watts, C. W., Shanahan, P., Dodd, I. C., Ober, E. S., Ashton, R. W., Webster, C.
 624 P., White, R. P. and Hawkesford, M. J.: Methods to estimate changes in soil water for phenotyping root
 625 activity in the field, , doi:10.1007/s11104-016-3161-1, 2017.

626 Wiese, T., Greenhalgh, S., Zhou, B., Greenhalgh, M. and Marescot, L.: Resistivity inversion in 2-D
 627 anisotropic media: numerical experiments, Geophys J Int, 201(1), 247–266, doi:10.1093/gji/ggv012,
 628 2015.

629 Wilderotter, O.: An adaptive numerical method for the Richards equation with root growth, Plant and
 630 Soil, 251(2), 255–267, doi:10.1023/A:1023031924963, 2003.

631 Wunderlich, T., Petersen, H., al Hagrey, S. A. and Rabbel, W.: Pedophysical models for resistivity and
 632 permittivity of partially water-saturated soils, Vadose Zone Journal, 12(4), doi:10.2136/vzj2013.01.0023,
 633 2013.

634 Zenone, T., Morelli, G., Teobaldelli, M., Fischanger, F., Matteucci, M., Sordini, M., Armani, A., Ferrè, C.,
 635 Chiti, T. and Seufert, G.: Preliminary use of ground-penetrating radar and electrical resistivity
 636 tomography to study tree roots in pine forests and poplar plantations, Functional plant biology FPB
 637 [online] Available from: <http://agris.fao.org/agris-search/search.do?recordID=US201301559026>
 638 (Accessed 14 September 2017), 2008.

639

Tables:

	θ_r [cm ³ cm ⁻³]	θ_s [cm ³ cm ⁻³]	a [1/cm]	n	K_s [cm/day]	λ
Sand	0	0.35	0.05	2	100.24	0.5
Loam	0.078	0.435	0.036	1.56	25	0.6

Table 1: Soil hydraulic properties. θ_r : Residual water content, θ_s : Saturated water content, a , n and λ : shape parameters in van Genuchten-Mualem equations, K_s : saturated soil hydraulic conductivity.

a) Sand without roots	Time:	Day 5	Day 10	Day 15	Day 18	Day 22
	σ_{bulkZ} [S/m]	0.0127	0.0074	0.0041	0.0015	0.0002
	σ_{bulkX} [S/m]	0.0215	0.0144	0.0106	0.0064	0.0012
	AF	1.68	1.93	2.58	4.26	6.24
b) Sand with roots	σ_{bulkZ} [S/m]	0.0128	0.0077	0.0045	0.0018	0.0002
	σ_{bulkX} [S/m]	0.0215	0.0144	0.0108	0.0066	0.0012
	AF	1.67	1.88	2.39	3.73	6
c) Loam without roots	σ_{bulkZ} [S/m]	0.0568	0.0449	0.0370	0.0279	0.0166
	σ_{bulkX} [S/m]	0.0594	0.0482	0.0417	0.0337	0.0190
	AF	1.04	1.07	1.12	1.19	1.14

d) Loam with roots	σ_{bulkZ} [S/m]	0.0566	0.0447	0.0369	0.0281	0.0170
	σ_{bulkX} [S/m]	0.0593	0.0481	0.0414	0.0334	0.0194
	AF	1.04	1.07	1.12	1.19	1.14

Table 2: Effective electrical conductivity in [S/m] and anisotropy factor at rhizotron scale computed using simulated plate electrodes at boundaries.

Figures:

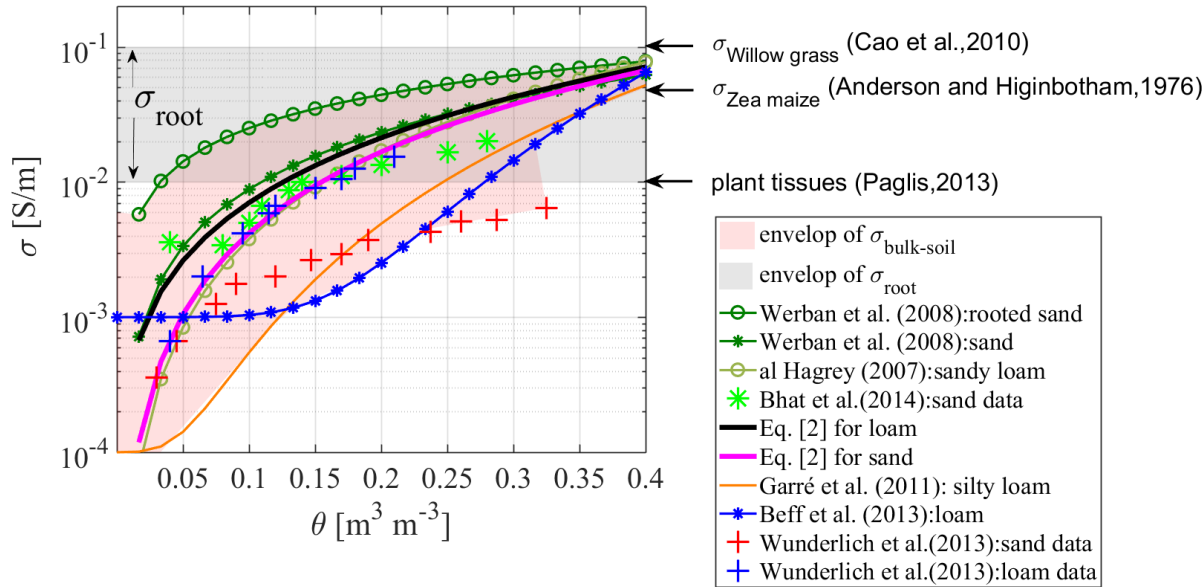


Figure 1. Comparison of soil and root electrical conductivity. The envelopes of σ_{soil} (some with and some without roots) and σ_{root} are shown as shaded areas.

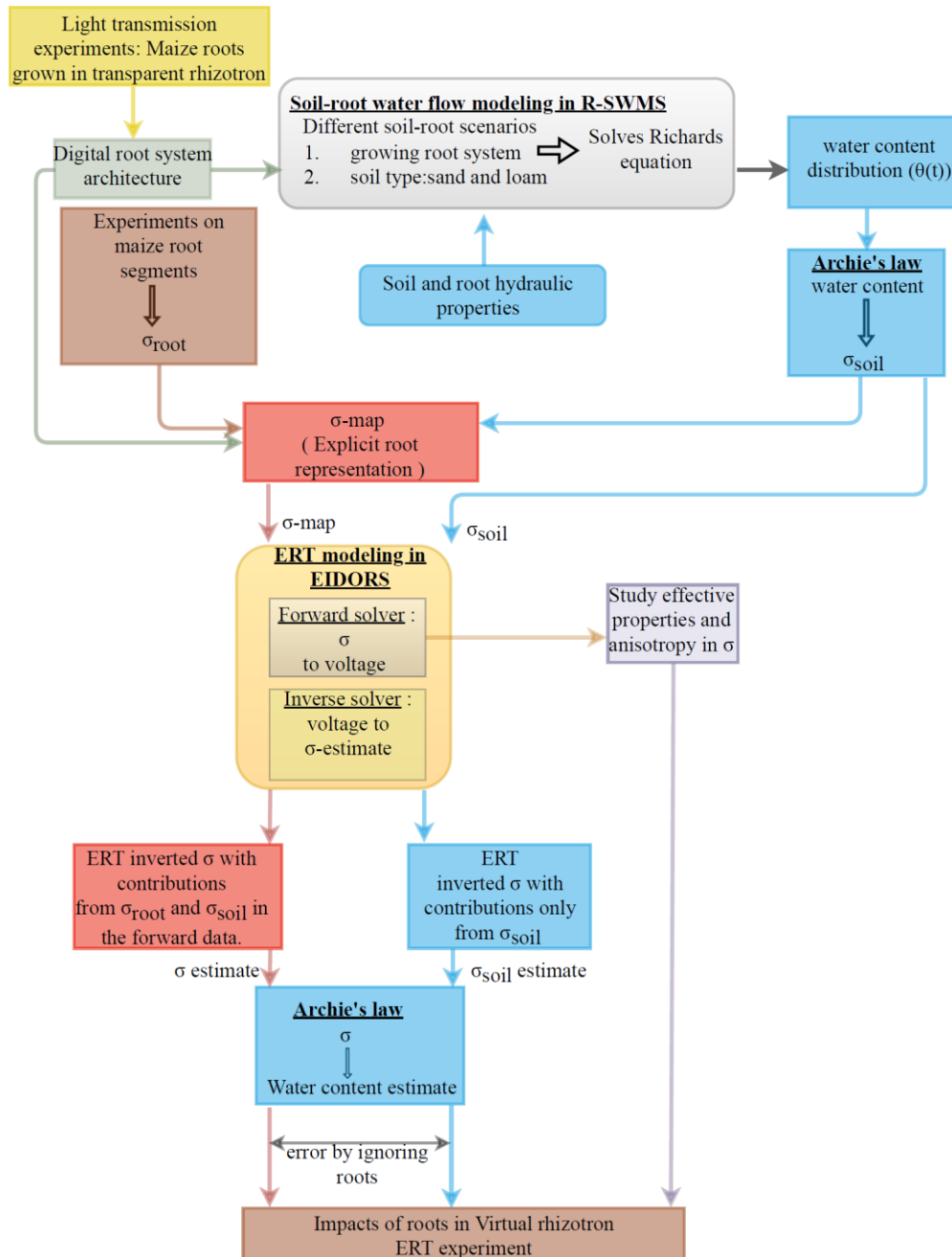


Figure 2: Flow chart for the simulation of Virtual Rhizotron drying experiment. First, a simulation of root water uptake and root growth of a maize plant in a rhizotron is run with a soil-plant water flow model (RSWMS, Javaux et al., 2008), which generates maps of soil water distribution (θ) and of root architecture evolution. Then these distributions are transformed into detailed electrical conductivity (σ) maps through bio/pedo-physical relations. Third, these distributions are used to simulate a virtual ERT measurement and inversion scheme to get a coarser distribution of σ estimates (see text for further details).

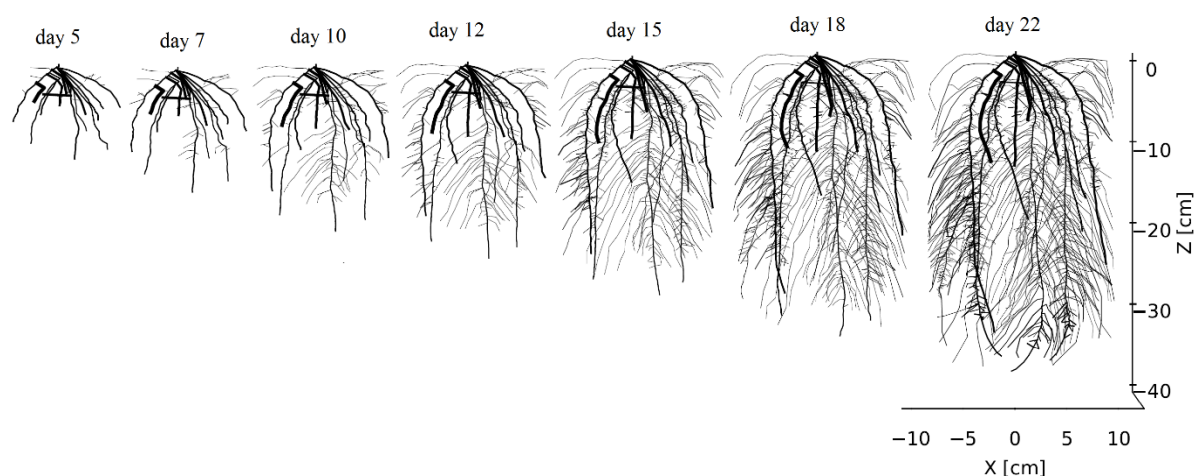


Figure 3: root architectural evolution shown at different times.

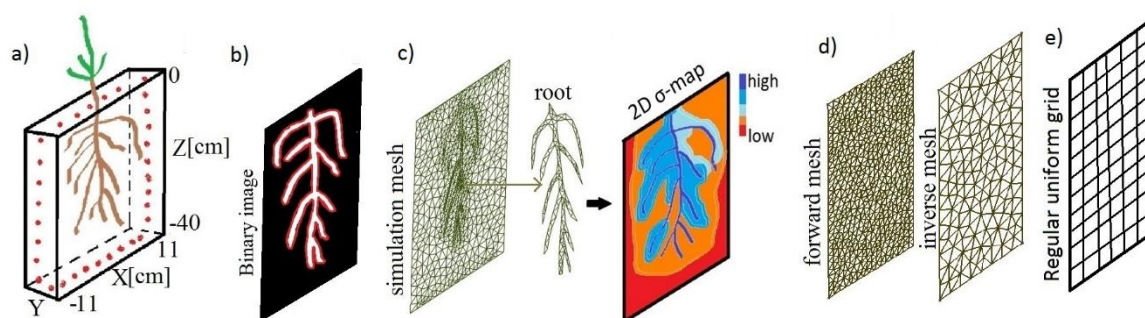


Figure 4: a) Virtual rhizotron schematic, b) binary image of schematic root architecture used to generate mesh. The red region represents the spline curve that envelops the root surface. c) Simulation model (SMDL): simulation mesh with explicit root architecture and schematic conductivity distribution map, d) forward model (FMDL): forward and inverse mesh, and e) regular uniform grid used to simulate Richards' equation.

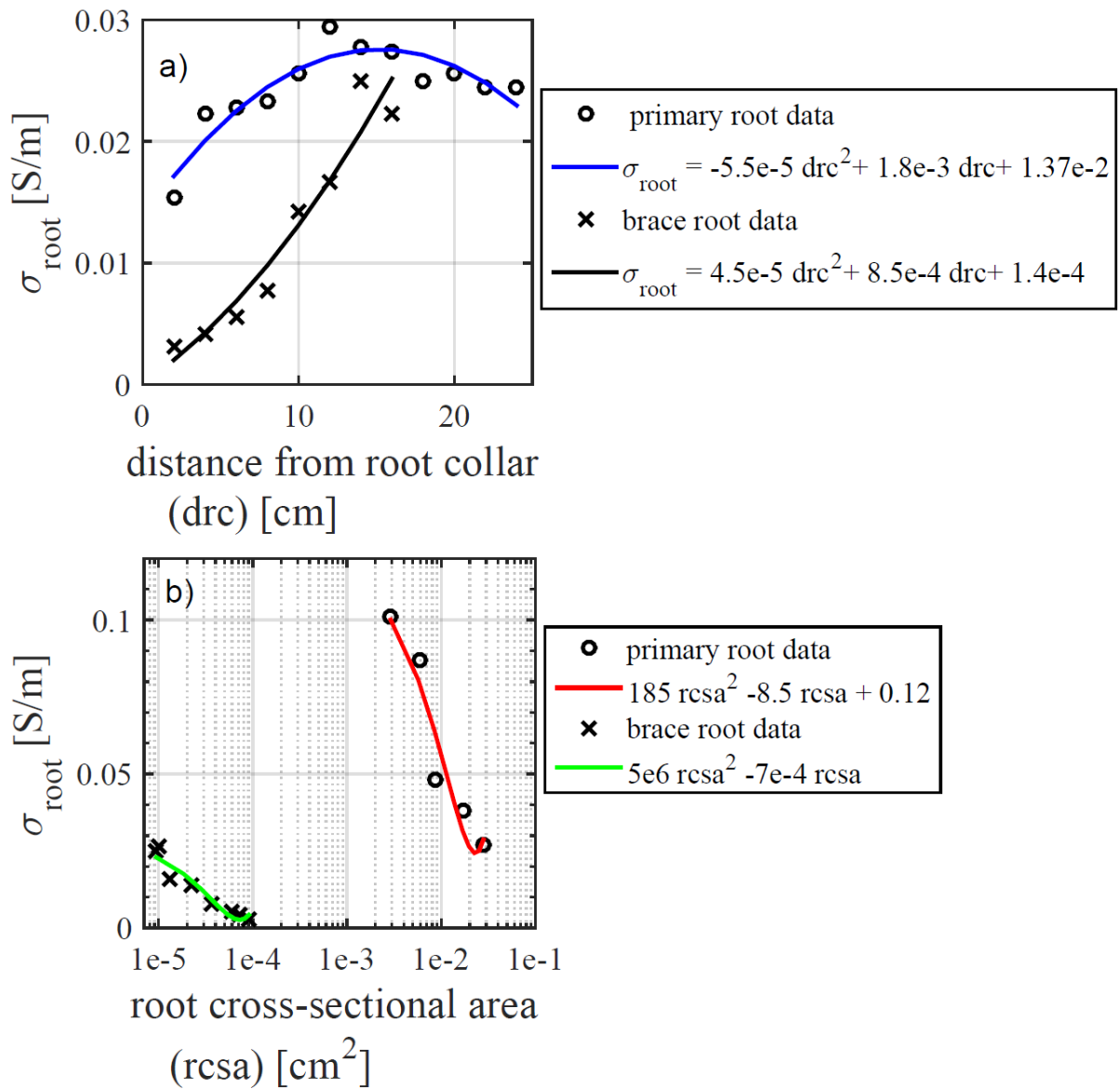


Figure 5: Measurement data on Maize roots a) σ_{root} vs distance from root collar, b) σ_{root} vs root cross sectional area. The quadratic fit is shown as solid line while measurement data is represented at discrete locations as circles (primary root) and crosses (brace root). The blue curve in Figure 5a is the data used in simulation model.

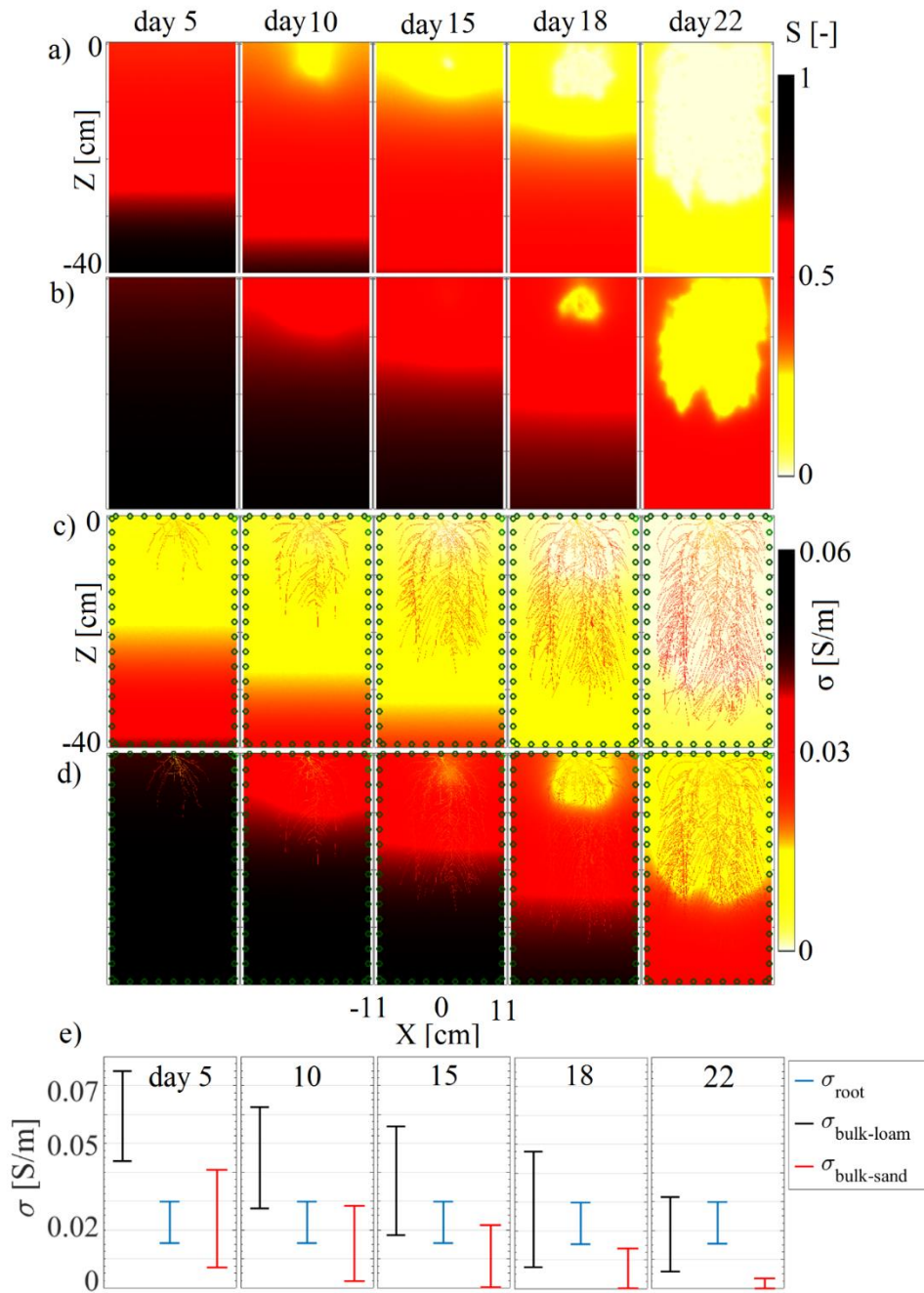


Figure 6: Volumetric water saturation distribution in a) sand and b) loam, and its corresponding σ -maps in c) sand and d) loam, e) variability of σ in the rhizotron at different times. The vertical bars at various times represent the minimum and maximum value of σ , respectively.

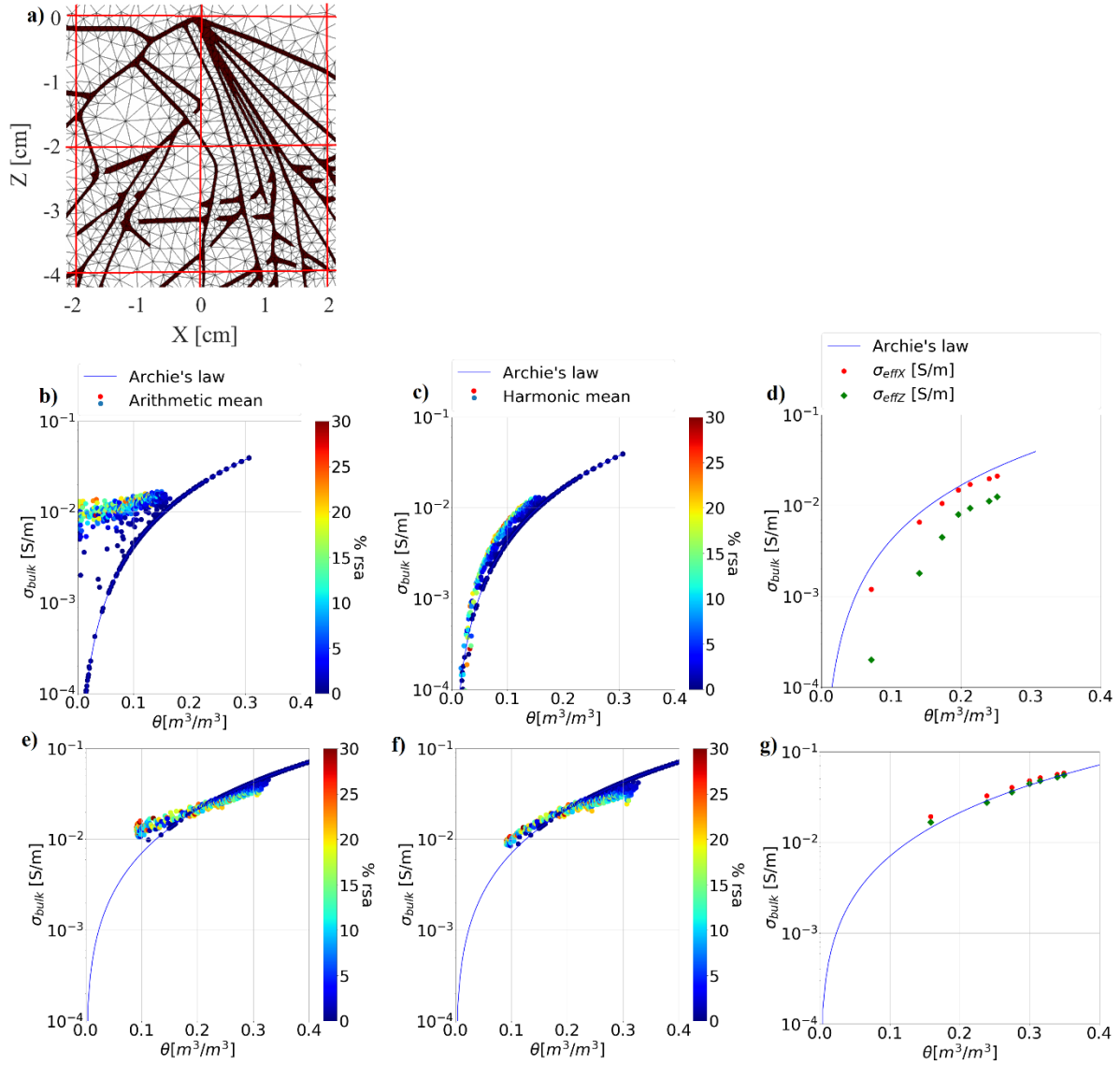


Figure 7: a) A section of the SMDL mesh with averaging blocks shown in red squares. The root elements are in brown color, b) Comparison of Archie's law with block-wise arithmetic averaged quantities ($\langle \sigma_{bulk} \rangle$ vs. $\langle \theta \rangle$) in sand, c) Comparison of Archie's law with block-wise harmonic averaged quantities ($\langle \sigma_{bulk} \rangle$ vs. $\langle \theta \rangle$) in sand, d) Comparison of Archie's law with rhizotron scale effective bulk property in sand, e) Comparison of Archie's law with block-wise arithmetic averaged quantities ($\langle \sigma_{bulk} \rangle$ vs. $\langle \theta \rangle$) in loam, f) Comparison of Archie's law with block-wise harmonic averaged quantities ($\langle \sigma_{bulk} \rangle$ vs. $\langle \theta \rangle$) in loam, g) Comparison of Archie's law with rhizotron scale effective bulk property in loam.

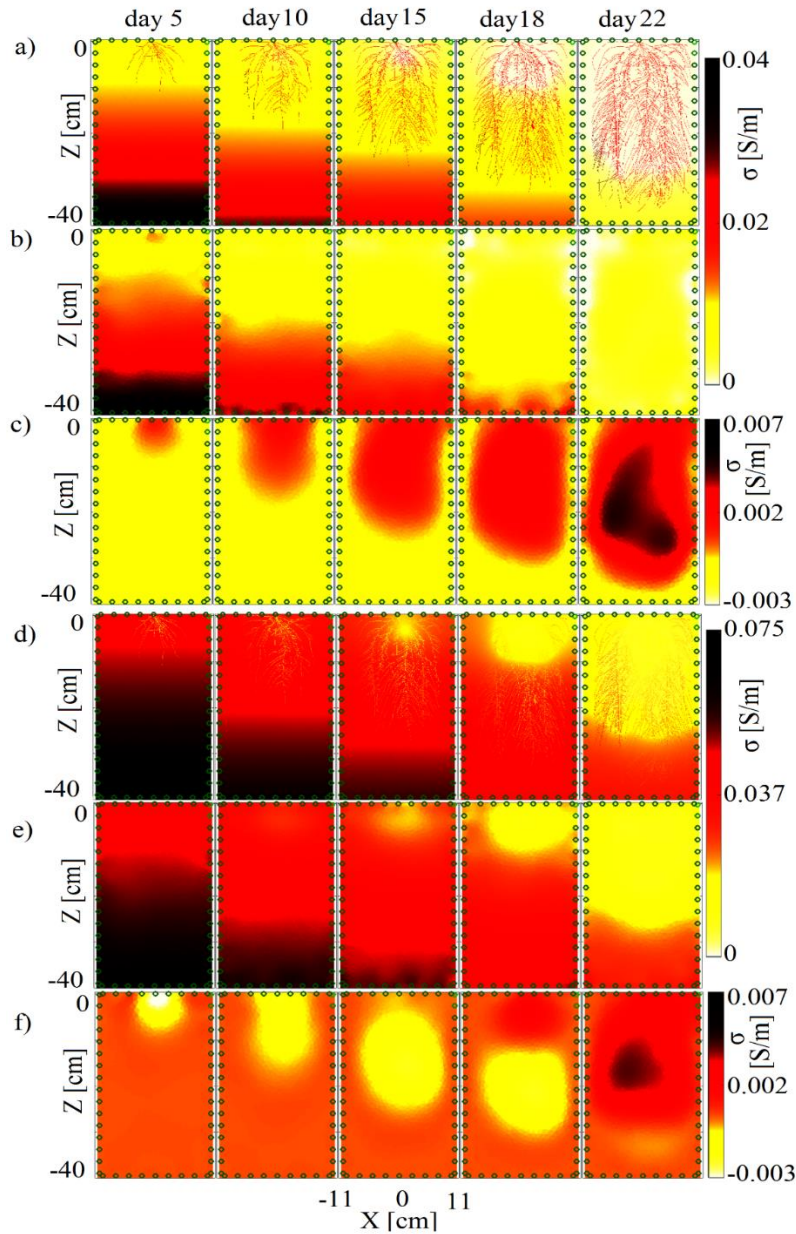


Figure 8: Sand: a) detailed electrical conductivity map of maize root at different times; b) tomography inversion with the root conductivity included in the forward model; c) difference between the inversions results with and without root conductivity accounted for in the forward model. Green circles represent the electrode positions. Loam: d) Conductivity map of maize root at different time; e) tomography inversion with the root conductivity included in the forward model; f) difference between the inversions results with and without root conductivity in the forward model.

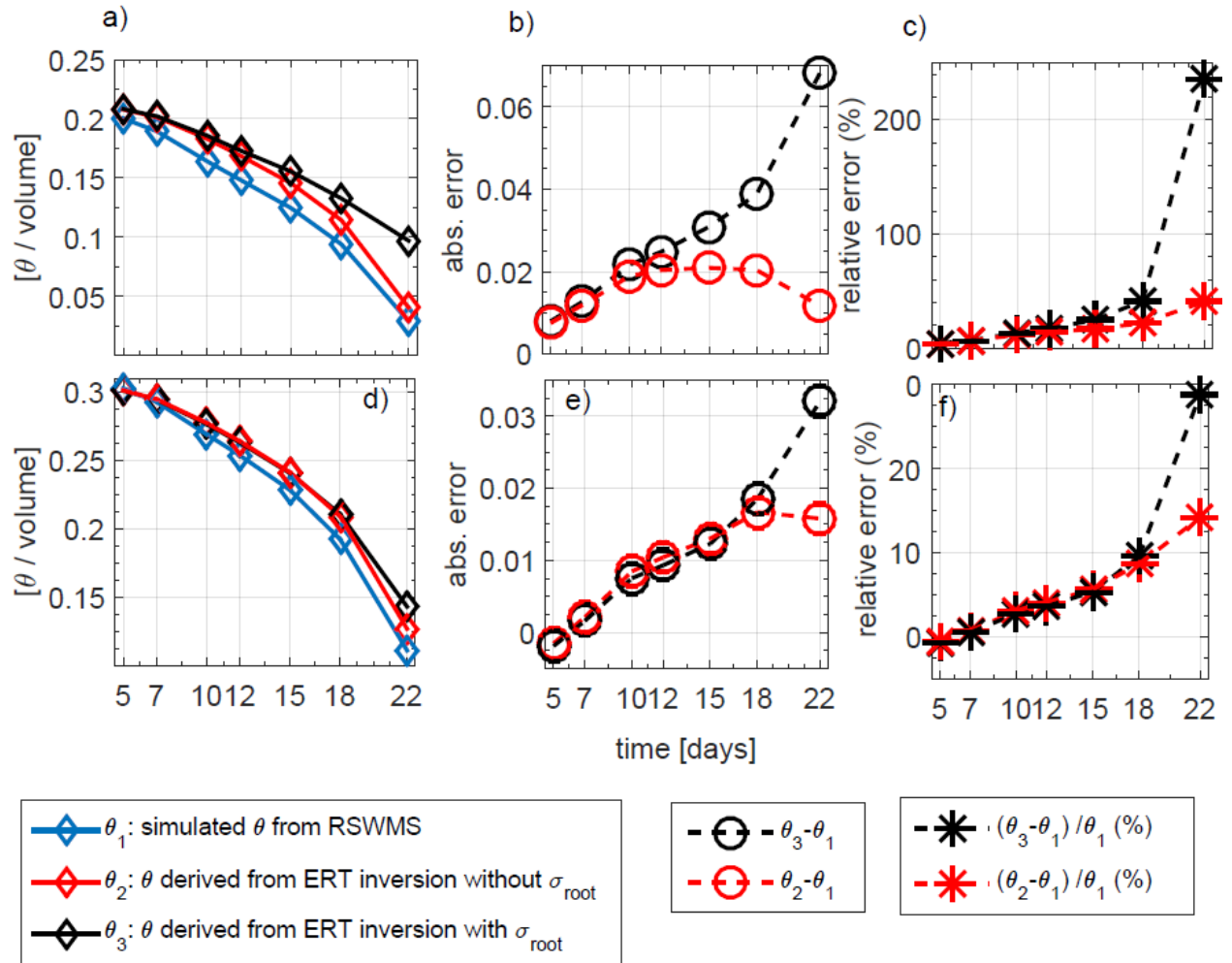


Figure 9: a) Comparison of normalized volume averaged water content, obtained from simulated SWC (denoted as θ_1) and ERT imaging without and with inclusion of σ_{root} denoted by θ_2 and θ_3 , respectively as a function of different root growth time in sand, b) Absolute error between (θ_1, θ_3) and (θ_1, θ_2) , c) relative percentage error between (θ_1, θ_3) and (θ_1, θ_2) . Figures 9 (d,e,f) same as 9 (a,b,c) but in loam medium.

712 **Appendix**

713 The list of symbols used in this paper:

Symbol	Description
θ	soil water content
θ_s	saturated water content, assumed to be equal to soil porosity
$\langle\theta\rangle$	water content computed using spatial averaging of finite element mesh
θ_1	volumetric average of water content from RSWMS simulation
θ_2	volumetric average of water content from ERT inverted σ -map without the root electrical properties in the ERT forward data
θ_3	volumetric average of water content from ERT inverted σ -map with the electrical properties of roots included in the ERT forward data
n	soil porosity
h	matric head
K	isotropic hydraulic conductivity
S	degree of water saturation
σ	electrical conductivity in general.
σ_{soil}	electrical conductivity of soil in general
$\sigma_{surface}$	surface electrical conductivity of soil solid particles
σ_{root}	electrical conductivity of root segment, which is a function of root type
σ_w	electrical conductivity of soil fluidic phase
$\langle\sigma_{bulk}\rangle$	bulk electrical conductivity computed using spatial averaging of finite element mesh
σ_{bulk}	bulk or effective electrical conductivity of a composite medium comprising of root and soil, computed using plate electrodes at boundary
$\sigma_{bulk-soil}$	bulk or effective electrical conductivity of soil medium without roots
$\sigma_{bulk-loam}$	bulk or effective electrical conductivity of loam medium without roots
$\sigma_{bulk-sand}$	bulk or effective electrical conductivity of sand medium without roots
σ_{bulkX}	effective electrical conductivity in horizontal direction
σ_{bulkZ}	effective electrical conductivity in vertical direction

714